Effect of Air Jet Splitting on the Elliptical Burner Inverse Diffusion Flame Characteristics: A Computational Study

Ahmed A. Mahgoub
Continuous Combustion Laboratory, Mechanical Power Engineering Department, Faculty of Engineering - Mataria, Helwan University

Eslam I. Mohamed
Continuous Combustion Laboratory, Mechanical Power Engineering Department, Faculty of Engineering - Mataria, Helwan University

Ahmed A. Adam
Interdisciplinary Graduate School of Engineering Sciences (IGSES), Kyushu University

Mohamed S. Mohamed Gamal
Continuous Combustion Laboratory, Mechanical Power Engineering Department, Faculty of Engineering - Mataria, Helwan University

他

https://doi.org/10.5109/7323256

出版情報：Proceedings of International Exchange and Innovation Conference on Engineering & Sciences (IEICES). 10, pp.148-155, 2024-10-17. International Exchange and Innovation Conference on Engineering & Sciences
バージョン：

Effect of Air Jet Splitting on the Elliptical Burner Inverse Diffusion Flame Characteristics: A Computational Study

Ahmed A. Mahgoub[1], Eslam I. Mohamed[1], Ahmed A. Adam[2,1], Mohamed S. Mohamed Gamal[1], Ahmed M. Abdulnaim[1], Ahmed H. Elkholy[1], Mohamed Elmously[1]
[1]Continuous Combustion Laboratory, Mechanical Power Engineering Department, Faculty of Engineering – Mataria, Helwan University, Cairo 11718, Egypt, [2]Interdisciplinary Graduate School of Engineering Sciences (IGSES), Kyushu University, Fukuoka, Japan.
Corresponding author email: ahmed_mahgoub93@m-eng.helwan.edu.eg

Abstract: *This computational study explores the effects of air jet splitting on the combustion characteristics of elliptical burner inverse diffusion flames (IDFs). The paper focuses on the impact of increasing the number of central air jets on flame aerodynamics, temperature distribution, and pollutant emissions. The study utilizes ANSYS CFX 2022 R1 software for simulation to examine configurations with single, double, and triple air jets while maintaining constant thermal input and inlet velocities. Results indicated that air jet splitting enhances fuel-air mixing, reduces soot formation, and optimizes combustion efficiency. There was a notable impact on the temperature distribution within the flame and on the concentrations of pollutants emitted. The results enhance our comprehension of IDFs with elliptical jets, highlighting their potential utility in energy and thermal processes. This work underscores the significance of jet interaction and aerodynamics in advancing the IDF combustion technology for sustainable utilization.*

Keywords: Inverse Diffusion Flame; Elliptical Burner; CFD; Multi-Jet Air Injection

1. INTRODUCTION

The configuration of an inverse diffusion flame (IDF) holds significant potential for improving combustion characteristics, which is crucial for energy conversion, power generation, and transportation. IDF represents a type of diffusion flame where the fuel is introduced in the annular region of a co-axial burner, being entrained by the air jet located in the center. Enhancing fuel entrainment and mixing by increasing the relative velocity between the air and fuel jets result in a partially premixed flame [1]. Furthermore, increasing the number of air jets and optimizing their interaction can lead to an enhanced homogeneous fuel-air mixing and improved entrainment. The central air jet effectively mixes with the fuel jets, creating a turbulent flame with improved reliability and heat transfer characteristics. Concurrently, ambient air surrounding the fuel jets is entrained into the combustion zone, facilitating more complete and cleaner combustion [2].

Non-premixed or diffusion flames, including IDFs, generally exhibit broader flammability limits compared to premixed flames. IDFs combine the advantages of both premixed and non-premixed diffusion flames regarding operational safety, pollutant emissions, flame stability, and reduced susceptibility to issues like lift-off and flashback. These attributes render IDF more sustainable than NDF, prompting extensive experimental and numerical studies in both domestic and industrial applications [3, 4].

Therefore, comprehensive research is essential to understand the complexities of combustion in IDFs. This includes studying the flame configurations, emitted pollutants, and the factors influencing the combustion. Investigations often analyze operating conditions, fuel characteristics, and flame stability, and implement strategies to optimize combustion efficiency. Various diagnostic techniques have been developed to gain a deeper understanding of flame structure [3-5].

Numerous experimental and theoretical studies have investigated the configuration of IDFs from various perspectives, including flame stability, appearance, and temperature distribution. For instance, Wu and Essenhigh [5] examined laminar methane IDFs, focusing on observed and predicted temperature and composition profiles of stable species along the flame's axis. They classified IDF methane flames into six types, with two representative flames covering over 50% of the distribution. These representative flames featured a parabolic primary blue combustion zone, with a yellow, tapered annular zone starting one-third above the blue zone's side, enclosing a dark area above the blue zone and remaining open at the top. Mikofski et al. [6] investigated the impacts of airflow rates alternatives on methane and ethylene IDF flames using laser fluorescence with theoretical scale assessments. Finding that Soot masked the reaction zone; OH-LIF showed taller flames and more soot in ethylene flames.

The multi-inverse diffusion flame, an adaptation of the conventional IDF, divides the outer fuel jet into several circumferential jets around the central air jet. Compared to the conventional IDF, the multi-fuel jet IDF shows more stability at very low Reynolds numbers [7]. Elbaz and Roberts [1] they used high-speed OH-PLIF images and 2D PIV measurements to analyze an IDF with circumferential methane jets. Concluding that the increase of the air to fuel velocity ration enhances fuel entrainment and improving mixing. Sze et al. [7] experimentally investigated the flame appearance, i.e., flame luminosity and visual dimensions, temperature distribution, and NOx emissions of the IDF with co-axial (CoA) and circumferentially arranged fuel ports (CAPs). It has been found that the CAP flame exhibited distinct entrainment and combustion zones, whereas the CoA flame resembled a typical diffusion flame. The CAP flame exhibited higher temperatures and more intense air-fuel mixing than the CoA flame, with both flames displaying bell-shaped nitrogen oxides emission index ($EINO_X$) curves; however, CAP peaked at a lower

equivalence ratio than CoA. Zhen et al. [2] explored the impact of nozzle length on multi-jet fuel burners, finding that shorter nozzles led to a shorter potential core and flame base. Barakat et al. [8] compared two CAP burner designs, one with single central air port and the other with multiple air port, concluding that the latter showed emissions reduction up to 70%.

Stelzner et al. [9] conducted experimental and computational studies on the rich methane IDF structure, while Patel and Shah [10] investigated flame appearance, length, temperature, and velocity profiles using both experimental and numerical methods at different air-fuel velocity ratios. It was observed that flame length and maximum temperature increased with higher fuel jet velocity, featuring distinct entrainment and combustion zones separated by a flame neck. Bhatia et al. [11] numerically analyzed the effects of oxygen enrichment and gravity on IDF and NDF flame structures. Dong et al. [12] optimized an innovative IDF for impingement heating, examining the effects of air and fuel port diameter ratios on flame structure and emissions.

The aerodynamics of the burner can significantly affect the combustion characteristics of IDFs. An elliptical burner, for instance, can reduce the NO concentrations compared to circular burners due to its ability to entrain more air from the surrounding environment [13]. The utilization of elliptical jets provides several advantages in controlling the spreading and entraining of the jet by adjusting the ellipse aspect ratio. Elliptical jets, as opposed to circular jets, produce unique mixing behaviors and flow patterns. This distinction arises from the formation of vortex pairs along the ellipse's major axis. Investigating elliptical IDFs is crucial, as it offers new insights into how jet shape influences the flame structure and combustion characteristics by changing the flow patterns.

On the other hand, in our recently published paper [14], we investigated the effects of early air injection jets on swirl-stabilized spray flames, a phenomenon known as air-assisted combustion. The key findings include the shortening of the visible flame length, and consequently the flame thermal length, a transition from diffusion combustion to partially premixed lean combustion, an enhancement in the degree of premixing, and an improvement in soot oxidation.

The selection of combustible fuel is crucial in optimizing the combustion process and its resultant effects. The increasing demand for sustainable fuels in thermal energy applications is driven by the limited availability and harmful environmental impacts of fossil fuels. Methane (CH_4) and liquefied petroleum gas (LPG) have emerged as promising alternatives due to their wide availability and versatility. Methane, in particular, offers the benefit of clean combustion, resulting in lower greenhouse gas emissions. While LPG is considered a bridging fuel in the transition to full dependence on renewable energy [15]. However, challenges persist regarding the storage, transportation, and prevention of leaks associated with methane [16, 17].

In this research, a numerical investigation is conducted on a jet inverse diffusion flame (JIDF) originating from an elliptical-shaped burner. The main objective is to acquire novel insights into how jet interactions influence the structure of the flame. The overall objective is to examine the effect of increasing the number of central air jets and their interactions on the elliptical IDFs combustion characteristics while keeping the same thermal input as well as fixed air and fuel velocities. The computational model used in the present investigation has been previously validated with experimental work on LPG/air flames [4]. This research advances our comprehension of elliptical JIDFs, highlighting their potential utility in thermal energy applications.

2. METHODOLOGY

This study utilizes computational fluid dynamics (CFD) to investigate the effect of splitting the core air jet on the characteristics of an unconfined, vertically oriented elliptical IDF. The employed computational model has been previously validated in Mahgoub et al. [4] for the same burner. This model demonstrated robust performance in alignment with experimental data, specifically in predicting flame temperatures. The validation process involved a comparative analysis of various turbulence and combustion models. The BSL EARSM turbulence model, when combined with the simplified LPG composition, was confirmed to offer a dependable framework for the simulation of elliptical JIDFs. The consistency of these findings underpins the credibility of the model, thereby justifying its application in the current research. The steady-state Reynolds-averaged Navier–Stokes (RANS) model has been utilized in this study using the commercial software ANSYS CFX 2022R1. The following subsections detail out the geometry preparation, mesh generation, and simulation setup, along with the implemented models for turbulence, combustion, and radiation.

2.1 Computational Domain

The original burner design utilizes two concentric streams: a central air stream and a coaxial outer fuel stream. The air stream is circular, while the outer fuel stream has an elliptical cross-section with a 2:1 aspect ratio (30 mm major axis, 15 mm minor axis), as shown in Fig. 1, see Refs. [4, 18] for more burner details.

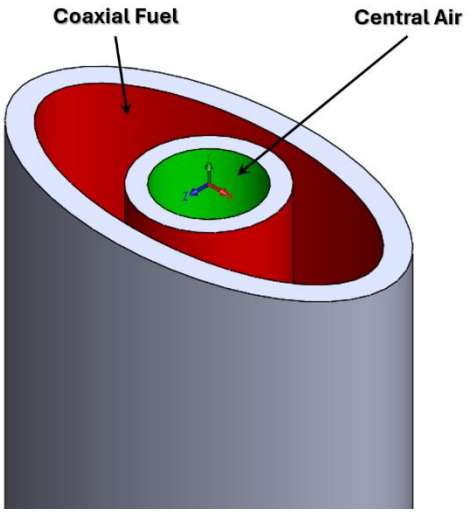

Fig. 1. The elliptical inverse diffusion burner.

To isolate the effects of air jet splitting on the flame structure, the core single air jet (Fig. 2-a) was divided into two (Fig. 2-b) and three (Fig. 2-c) separate jets while maintaining the same total equivalent area and mass flow rate for both air and fuel streams. This ensures identical inlet velocities for all configurations, as well as eliminating any influence from inlet geometry variations on the inlet flow momentum.

The central air jet diameter varies depending on the

number of jets: 8 mm for a single jet, 5.7 mm for double jets, and 4.6 mm for triple jets. The computational domain encompasses a height of 750 mm and a width of 200 mm.

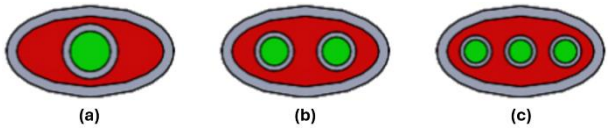

Fig. 2. The three burner configurations with central air jet splitting modes: (a) single, (b) double, and (c) triple.

To reduce the computational complexity, the quarter of the domain is only modeled, utilizing the major and minor planes of the fuel ellipse as symmetry planes (Fig. 3). Additionally, the burner upstream region is excluded due to its simple inlet geometry without complicated internal features.

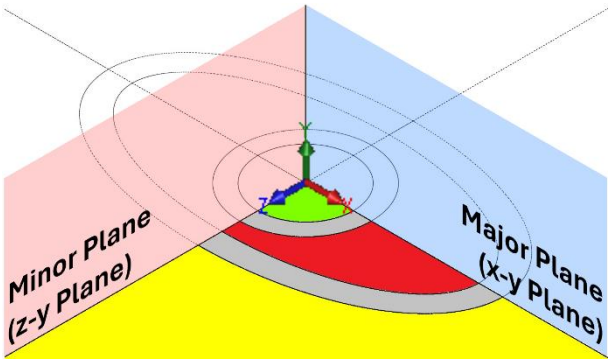

Fig. 3. Computational domain simplification (single air jet model).

2.2 Mesh Generation

Hexahedral computational meshes were generated using the Multizone method within ANSYS Meshing. Face sizing was applied to the inlet and wall faces at the domain bottom, with an element size of 0.2 mm. To achieve mesh densification near the domain bottom, edge sizing was applied to the domain axis with 300 divisions and a bias factor of 60. A mesh sensitivity analysis was conducted to validate the independence of the results from the mesh size. The analysis began with a face sizing featuring a large element size of 1 mm and applied edge sizing to the domain axis with 100 divisions and a bias factor of 20. These mesh settings were considered satisfactory for accurate model predictions, as further refinement of the mesh size resulted in only about a 1% variation in the computed values compared to the previous mesh configuration. The final mesh settings comprised 3.3 million elements and exhibited a skewness of 0.7, the highest values among the three models analyzed. Refer to Fig. 4 for a sample of the generated mesh for the single air jet model.

2.3 Simulation Setup

In order to simulate the experimental test case from the previous work of Mahgoub et al. [18] with a single air jet, the computational domain was assumed to operate under atmospheric conditions, and the lowest air jet velocity was selected, as the worst case regarding the air/fuel mixing and soot formation. The air and fuel normal velocities were set at 13.26 m/s and 0.026 m/s, respectively, in all simulated cases. This air jet velocity resulted in Reynolds numbers of 6752, 4811, and 3882, for single, double, and triple air jet, respectively.

The major and minor sides of the domain were assigned as a Symmetry boundary condition. The outer side of the domain was set as an opening to atmospheric air. The bottom of the domain utilized an opening boundary condition with entrainment of mass and momentum, and a zero-gradient turbulence option. Finally, the upper face of the domain was assigned as an outlet boundary condition with zero average static pressure.

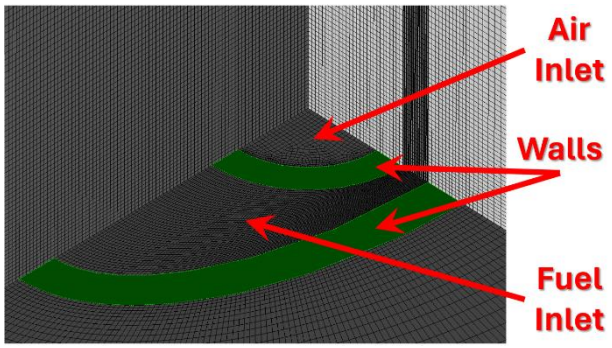

Fig. 4. A 3D snapshot of the generated mesh (single air jet model).

2.4 Simulation Models

The Baseline Explicit Algebraic Reynolds Stress Model (BSL EARSM) is utilized in this study. While the BSL EARSM is a type of Reynolds Stress Model (RSM) that offers a more detailed description of turbulence anisotropy (varying turbulence intensity in different directions) by solving transport equations for each individual Reynolds stress component [19]. It excels in predicting separation onset and flows with complex geometries and strong adverse pressure gradients. However, due to the additional equations it solves, BSL EARSM can be computationally more expensive than simpler models. Our previous study [4] compared BSL EARSM to the k-ε model, demonstrating the superiority of BSL EARSM for simulating the IDF of the elliptic burner.

The governing equations for the BSL EARSM turbulence model are derived from the Reynolds-averaged Navier-Stokes (RANS) equations and typically include the following [20]:

Transport equation for turbulent kinetic energy (k):

$$\frac{\delta k}{\delta t} + U \cdot \nabla k = P_k - \beta^* k w + \nabla \cdot \left[\left(v + \frac{v_t}{\sigma_k} \right) \nabla k \right]$$

Transport equation for specific dissipation rate (ω):

$$\cdot \nabla \omega = \alpha \frac{\omega}{k} P_k - \beta \omega^2 + \nabla \cdot \left[\left(v + \frac{v_t}{\sigma_\omega} \right) \nabla \omega \right] + 2(1 - F_1) \frac{\sigma_{\omega 2}}{\omega} \nabla k \cdot$$

where α, β, σ_ω, $\sigma_{\omega 2}$, and F_1 are model constants and functions.

Explicit Algebraic Reynolds Stress Model:

The Reynolds stress tensor $R = \underline{u_i' u_j'}$ is modeled using an explicit algebraic relation derived from the Reynolds stress transport equations. This involves a nonlinear

relationship between the Reynolds stresses and the strain and rotation rates of the mean flow.
The Reynolds stress tensor components are approximated as:

$$\boldsymbol{R = 2kA}$$

where A is a function of the strain rate tensor S and the rotation rate tensor Ω.
Turbulent viscosity (v_t):
The turbulent viscosity is defined as:

$$\boldsymbol{v_t = \frac{k}{\omega}}$$

The study also utilizes the Eddy Dissipation Model (EDM) due to its flexibility in incorporating user-defined reactions and materials without limitations from pre-existing libraries. However, a key limitation of EDM lies in its accuracy for predicting intermediate species like CO. This stems from the model's inherent assumption of near-complete combustion. Consequently, EDM often overestimates both the CO_2 emissions and adiabatic flame temperature, while underestimating CO formation, particularly in fuel-rich and near-stoichiometric regions.
In radiative transfer simulations, the choice of model depends on the desired balance between accuracy and computational efficiency. The discrete transfer model (DTM) was adopted for spatial discretization due to its high efficiency, while gray model was selected for the spectral approximation.
For a detailed explanation of the governing equations employed by the utilized models, please refer to Mahgoub et al. [4].

3. RESULTS AND DESCUSSIONS

3.1 Aerodynamics and Flow Patterns

The impact of splitting the central air jet on the flow field of the IDF is illustrated in Fig. 5. The figure shows the results of three models: single, double, and triple air jet injection. It presents velocity vectors superimposed on velocity magnitude (*U*) contours for both major and minor planes, specifically highlighting the flow fields surrounding the flame base. The velocity magnitude (*U*) is the resultant of the three velocity components, *u*, *v*, and *w*, and is given by the formula:

$$\boldsymbol{U = \sqrt{(u^2 + v^2 + w^2)}}$$

The vectors depicted on each plane represent the tangential vectors to the plane, meaning they are the projections of the resultant vector onto the plane.
A comparative analysis of the flow entrainment towards the air jets reveals that increasing the number of air jets increases the velocity magnitude and prompts the velocity vectors to deflect and merge with the air jets at an earlier stage, as indicated by the two white arrows in Fig. 5 (c). The enhanced air entrainment, facilitated by the division of the air jet, is indicative of improved fuel entrainment. This phenomenon promotes more effective fuel-air mixing, leading to a reduction in soot formation.
The underlying mechanism is attributed to the augmented fuel-air jet interfacial area of entrainment and mixing due to air jet splitting. Additionally, the overall entrainment is bolstered by the jet interaction effects. An expanded turbulence scale further contributes to this behavior by providing more space for creating and operating the entrainment vortices, thereby drawing larger reactive masses together and facilitating faster soot oxidation rates, leading to more efficient combustion.
Similar observations have been reported in previous research employing a multi-hole central air injector, where a reduction in soot was noticed when transitioning from a single to a multi-hole air jet configuration [8].

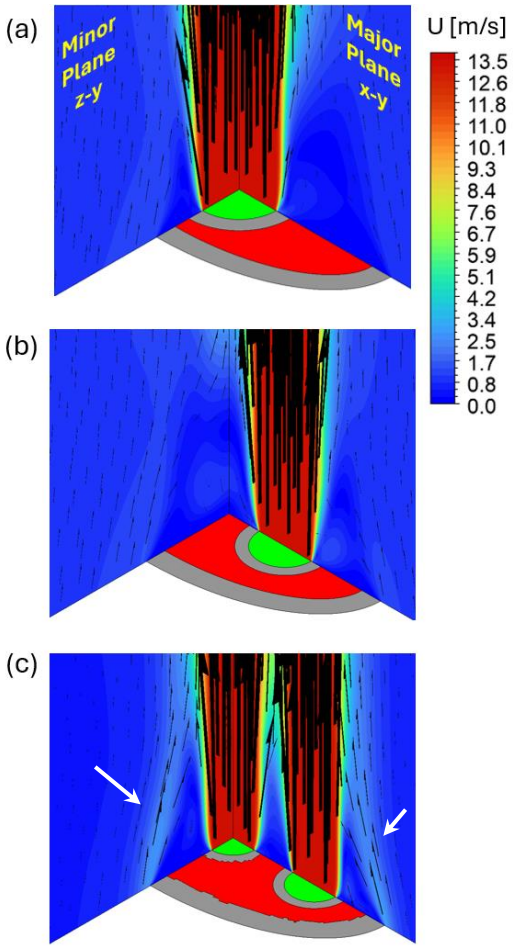

Fig. 5. Velocity vectors superimposed on velocity magnitude (*U*) contours for both major and minor planes; (a) single, (b) double, and (c) triple air jet injection.

To gain deeper insights into the effect of air jet splitting on the entrainment of both the fuel and the surrounding atmospheric air, Fig. 6 illustrates the radial entrainment, which is presenting by velocity vectors superimposed on velocity magnitude contours for a horizontal plane 3 mm above the burner exit plane.
In the case of a single air jet (Fig. 6 (a)), the entrainment is evidently weak, with the airflow dispersing away from the jet, indicating a jet expansion process. The small vectors directed towards the center of the burner suggest a minimal fuel and ambient air intake into the central air jet, especially at both sides of the major axis (revealed by the two white arrows in Fig. 6 (a)). Which interprets the formation of the soot crescents in the same region as seen in the flame images in the prior experimental study [18].
When the air jet is split into two separate jets (Fig. 6 (b)), the vectors increase in size, particularly on the left and right sides, indicating enhanced entrainment. Additionally, the two air jets expand outward while forming a negative pressure zone between them, demonstrating improved entrainment due to jet interaction.
The utilization of a triple air jet configuration (Fig. 6 (c))

maximizes the entrainment, as shown by both the velocity contours and vectors. The interaction of the flows in this configuration results in a deflection of the outer jets inward, toward the middle jet, creating a swirl-like motion (indicated by the two white arrows in Fig. 6 (c)). This motion ensures better mixing in the early mixing zone of the flame, enhancing fuel entrainment and consequently promoting soot oxidation.

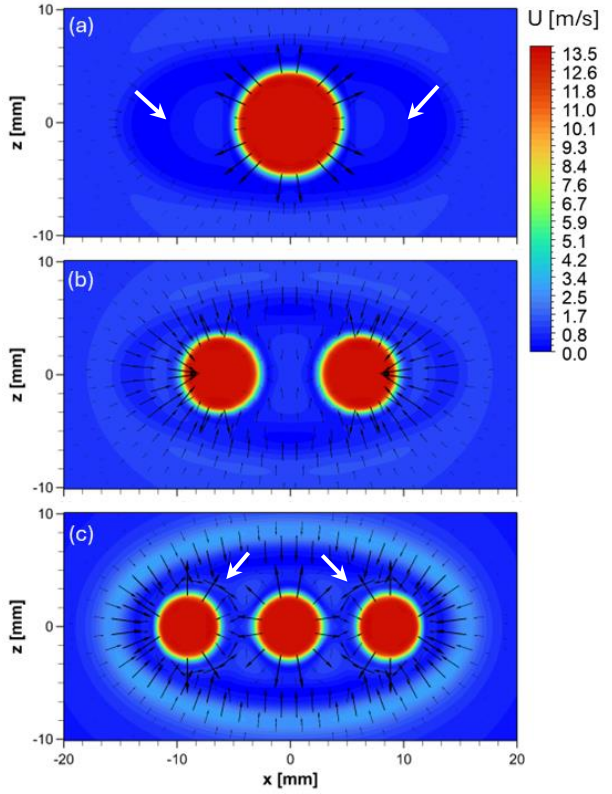

Fig. 6. Velocity vectors superimposed on velocity magnitude (*U*) contours for a horizontal plane 3 mm above burner rim for single (a), double (b), and triple (c) air jet configurations.

3.2 Temperature Field

Fig. 7 and Fig. 8 present the temperature contours on both the major and minor planes for single, double, and triple air jet injection. Our previous research [4] identified four essential and consecutive zones in the thermal structure of an IDF issued from the examined elliptical burner: the entrainment zone (flame base), the merging zone, the main reaction zone, and the post-combustion zone. Below, it is explained the effect of air jet splitting on these different zones within the flame's thermal structure.

In the early region ($0 < y < 30$ mm) of the single air jet flame (Fig. 7(a) and Fig. 8(a)), which encompasses the entrainment and merging zones, fresh and cold reactants result in a relatively cool flame base. As the flame progresses into the merging zone, the temperatures gradually increased due to ongoing chemical reactions, reaching their peak in the main reaction zone.

When the air jet splits into two or three jets, the entrainment is enhanced, and the entrained fuel is more evenly distributed among the air jets. Hence, the three jets result in multiple parallel, thinner hot regions rather than a single thick hot region seen in the single air jet flame. Additionally, increasing the number of air jets reduces the gap between the air jet and the fuel elliptical port edge in the major direction, which enhancing the fuel entrainment and reducing the soot crescent around the flame base (formed by a normal diffusion flame mode) by boosting the reaction and increasing temperatures in this region, as indicated by the white arrows in Fig. 7. Conversely, increasing the number of air jets simultaneously increases the gap in the minor direction, allowing the flame neck to enlarge in the minor direction (see the white arrows in Fig. 8).

In the main reaction zone ($50 > y \geq 30$ mm) of the single air jet flame (Fig. 7(a) and Fig. 8(a)), the highest temperature is achieved due to the highest heat release, resulting in high temperature gradients indicated by denser contour levels. Splitting the air jet affects this region by reducing both the width and height of the main reaction zone because of the early fuel consumption in the previous zones, which is caused by enhanced entrainment and mixing (indicated by the red arrows in Fig. 7 and Fig. 8).

It is worth noting that the minor plane temperature distribution for the double-jet configuration shown in Fig. 8(b) appears slightly vague, as it shows an enlarged reaction zone compared to the other configurations. This is misleading, as the double-jet configuration is characterized by having a core free from a central air jet, resulting in a hotter flame core.

In the post-combustion zone ($y > 50$ mm) of the single-jet model (Fig. 7(a) and Fig. 8(a)), temperatures are gradually decreased due to the completion of the reaction with all fuel consumed in the main reaction zone, and due to the consumption of atmospheric air. Increasing the number of air jets enhances the entrainment of ambient air, which in turn maximizes the reduction of temperatures in the post-combustion zone, as indicated by the black arrows in Fig. 7 and Fig. 8.

3.3 Pollutants Concentrations

The computed CO mass fraction contours (Fig. 9 and Fig. 10) accurately replicate the flame thermal structure. As shown in these figures, the CO concentration is increased along the curved path of the traveling flow before being fully oxidized near the air jets. This behavior is analogous to previous experimental results obtained with a single air jet [18], which showed the presence of a soot crescent on both fuel-rich sides of the major axis of the fuel elliptical port around the flame neck.

Increasing the number of air jets evidently enhances the air-fuel mixing, which is reflected in the rapid CO oxidation on both major and minor planes. This behavior may also affect the soot formation and oxidation in the region of the soot crescent, as depicted in a previous experimental study using a multi-hole central air injector [8].

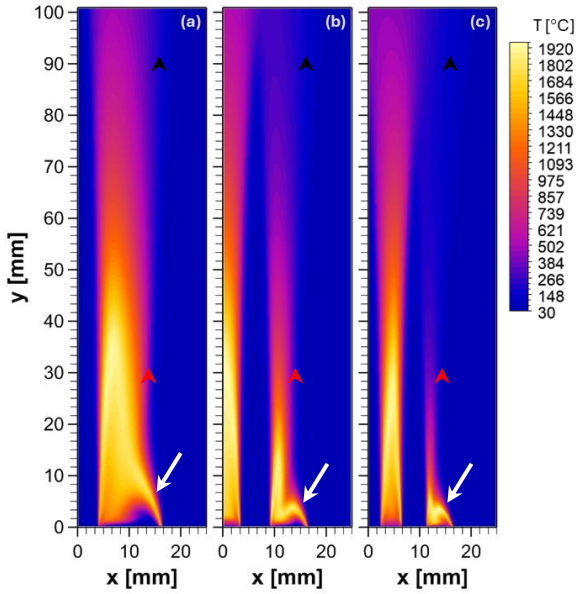

Fig. 7. Temperature contours on the major plane for (a) single, (b) double, and (c) triple air jet.

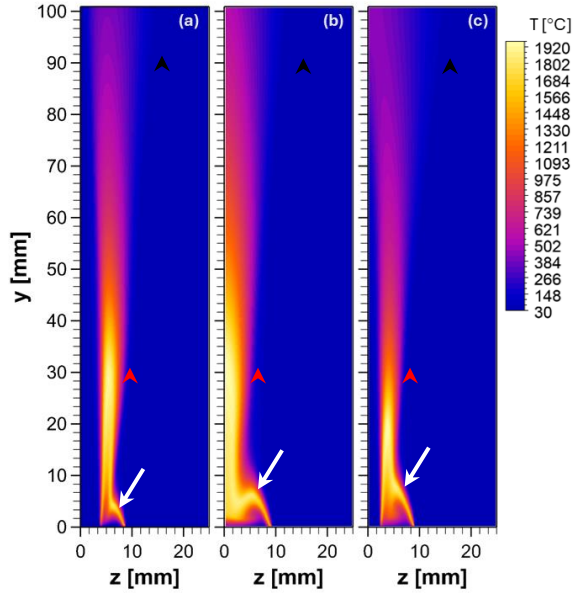

Fig. 8. Temperature contours on the minor plane for (a) single, (b) double, and (c) triple air jet.

The fuel flow deflection towards the air jet exhibits distinct behavior between the major and minor planes. In the major plane, raising the number of air jets leads to a reduction in the gap between the air jets and the most distant vertex on the major axis of the fuel ellipse, thereby decreasing the fuel deflection in the major plane (white arrow in Fig. 9). Conversely, in the minor plane, as the number of air jets increases, their diameters decrease to maintain a constant total area. While these results lead to an increased gap between the central air jet and the most distant vertex on the minor axis of the fuel ellipse, leading to greater fuel deflection towards the central air jet (white arrow in Fig. 10). Although a larger fuel deflection indicates higher concentrations of CO and soot, the overall major and minor fuel deflections are decreased as the number of air jets increases. This observation supports the hypothesis that increasing the number of air jets helps to maintain the structure of the IDF at low air jet velocities.

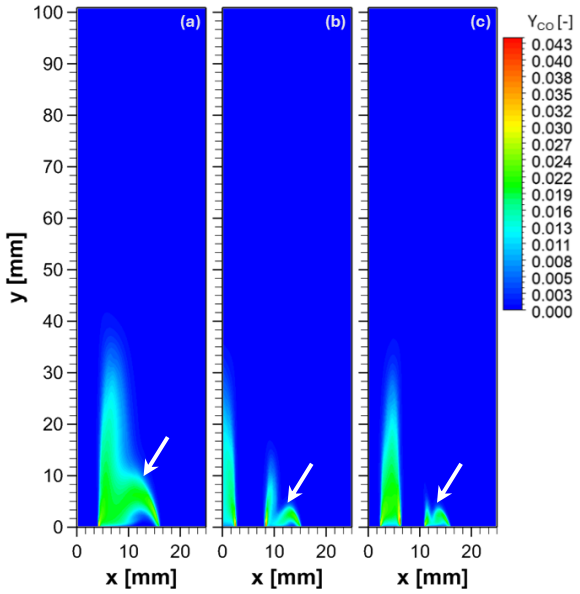

Fig. 9. CO mass fraction contours on the major plane for (a) single, (b) double, and (c) triple air jet.

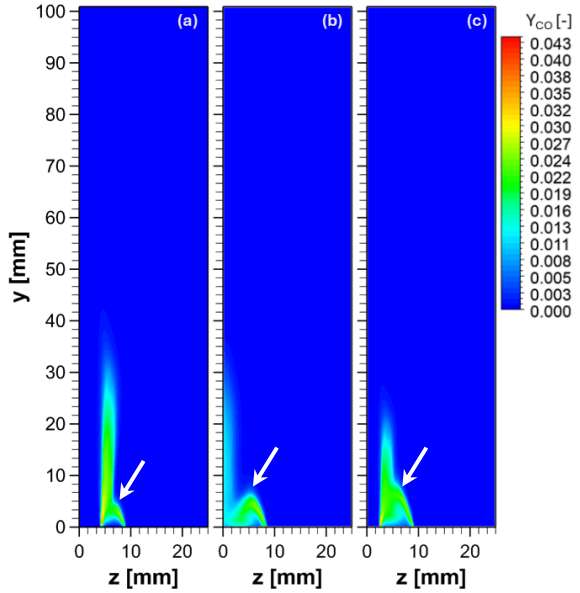

Fig. 10. CO mass fraction contours on the minor plane for (a) single, (b) double, and (c) triple air jet.

The concentrations of nitric oxide (NO) are intrinsically linked to the thermal structures of the flames, as illustrated in Fig. 11 and Fig. 12. The peak NO concentrations are observed in the main reaction zones of each flame, corresponding to the regions of maximum temperature. The formation of thermal NO depends on both the availability of air within the flame and the maximum temperature achieved. Thus, modulating the maximum flame temperature and its spatial distribution can significantly impact both the peak and overall thermal NO concentrations. Whilst this modulation is effectively achieved through air jet splitting, as demonstrated in Fig. 11 and Fig. 12.

In the case of a single air jet flame, a large volume of high temperatures, coupled with a high availability of air, results in an extensive thermal NO volume with relatively higher concentrations (Fig. 11(a) and Fig. 12(a)). However, increasing the number of air jets to two and three reduces the volume of high-temperature regions with a high availability of air, leading to leaner conditions. Consequently, both the volume and

concentration of NO are reduced, as shown in Fig. 11(b, c) and Fig. 12(b, c).

This reduction can also be ascribed to the improved fuel entrainment and mixing facilitated by the increased number of air jets. This process consumes the fuel earlier in the flame, particularly in the initial reaction zones ($0 < y < 20$ mm), where excess air is limited in the high-temperature regions. As a result, lower NO is produced in these early reaction zones, as indicated by the white arrows in Fig. 11. Additionally, the downstream air-rich zones ($y > 20$ mm) are maintained at lower temperatures, further reducing the thermal NO production in these areas.

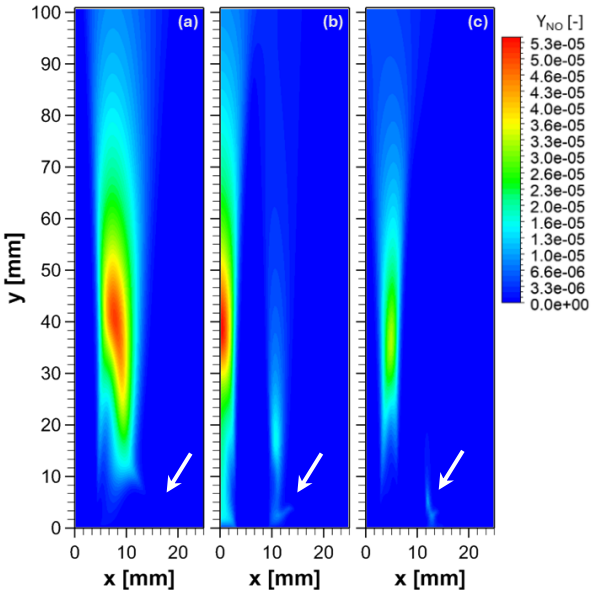

Fig. 11. NO mass fraction contours on the major plane for (a) single, (b) double, and (c) triple air jet.

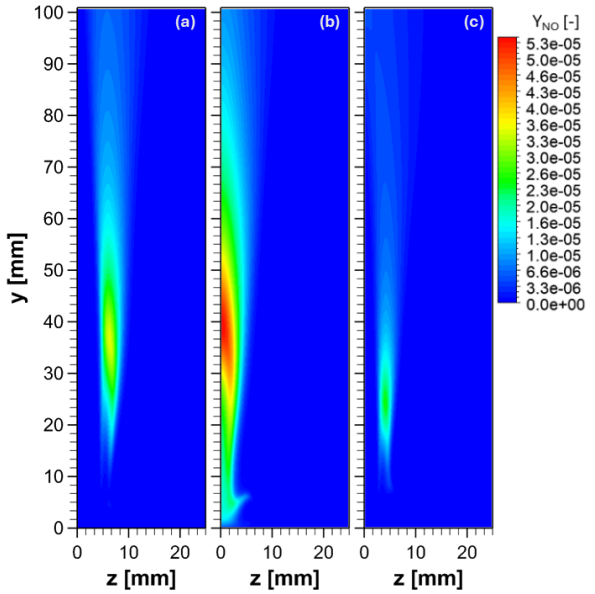

Fig. 12. NO mass fraction contours on the minor plane for (a) single, (b) double, and (c) triple air jet.

4. CONCLUSION

The study presents a detailed computational fluid dynamics (CFD) analysis of the impact of air jet splitting on the jet inverse diffusion flames (JIDFs) combustion characteristics with an elliptical burner. The simulations were conducted using ANSYS CFX 2022 R1, employing various models to investigate the aerodynamics, temperature fields, and pollutant concentrations of single, double, and triple air-jet IDFs, while maintaining constant thermal input and inlet velocities. The principal conclusions of this research are summarized as follows:

- Enhanced fuel-air mixing: Splitting the central air jet into multiple jets significantly enhances the entrainment of fuel and ambient air. This improvement in the fuel-air mixing leads to a reduction in soot formation and achieves more efficient combustion.
- Velocity modulation and flow patterns: The introduction of multiple air jets modulates the velocity magnitude and alters flow patterns due to jet interactions. This results in the earlier merging of fuel and ambient air with the air jets, thereby increasing the entrainment velocity.
- Optimized combustion zone: Transitioning from a single to a multi-air-jet configuration causes a contraction of the main combustion zone. While this shrinkage is attributed to the early consumption of fuel in the entrainment and mixing region, which is essential for optimizing the combustion process.
- Reduction in pollutant emissions: A significant reduction in the emissions of pollutants such as carbon monoxide (CO) and nitric oxides (NO) is observed. Which indicates that the air jet splitting technique for IDFs is a promising method for achieving cleaner combustion in practical applications.

These findings suggest that the approach employed in this study could lead to substantial improvements in the combustion efficiency and emissions control of IDFs. Such advancements are critical for promoting environmental sustainability and energy conservation.

5. REFERENCES

[1] Elbaz, A.M. and Roberts, W.L., Flame structure of methane inverse diffusion flame, Experimental Thermal and Fluid Science 56 (2014) 23-32.

[2] Zhen, H.S., Choy, Y.S., Leung, C.W., and Cheung, C.S., Effects of nozzle length on flame and emission behaviors of multi-fuel-jet inverse diffusion flame burner, Applied Energy 88(9) (2011) 2917-2924.

[3] Zhen, H.S., Leung, C.W., and Cheung, C.S., Thermal and emission characteristics of a turbulent swirling inverse diffusion flame, International Journal of Heat and Mass Transfer 53(5-6) (2010) 902-909.

[4] Mahgoub, A.A., Gamal, M.S.M., and Abdulnaim, A.M., Numerical Study of Jet Inverse Diffusion Flames Issuing from an Elliptical Burner, Proceedings of International Exchange and Innovation Conference on Engineering & Sciences (IEICES) 9 (2023) 397-404.

[5] Wu, K.-T. and Essenhigh, R.H., Mapping and structure of inverse diffusion flames of methane, Symposium (International) on Combustion 20(1) (1985) 1925-1932.

[6] Mikofski, M.A., Williams, T.C., Shaddix, C.R., and Blevins, L.G., Effect of Varied Air Flow on Flame Structure of Laminar Inverse Diffusion Flames, in 2004 Spring Meeting, Western States Section /The Combustion Institute. 2004: United States.

[7] Sze, L.K., Cheung, C.S., and Leung, C.W., Appearance, temperature, and NOx emission of two

inverse diffusion flames with different port design, Combustion and Flame 144(1-2) (2006) 237-248.
[8] Barakat, H.Z., Kamal, M.M., Saad, H.E., and Eldeeb, W.A., Performance enhancement of inverse diffusion flame burners with distributed ports, Proceedings of the Institution of Mechanical Engineers, Part A: Journal of Power and Energy 229(2) (2014) 160-175.
[9] Stelzner, B., Hunger, F., Voss, S., Keller, J., Hasse, C., and Trimis, D., Experimental and numerical study of rich inverse diffusion flame structure, Proceedings of the Combustion Institute 34(1) (2013) 1045-1055.
[10] Shah, R., Experimental and Numerical Investigation of LPG-Fueled Inverse Diffusion Flame in a Coaxial Burner, International Journal of Advanced Thermofluid Research 3(1) (2017) 16-28.
[11] Bhatia, P., Katta, V.R., Krishnan, S.S., Zheng, Y., Sunderland, P.B., and Gore, J.P., Simulations of normal and inverse laminar diffusion flames under oxygen enhancement and gravity variation, Combustion Theory and Modelling 16(5) (2012) 774-798.
[12] Dong, L.L., Cheung, C.S., and Leung, C.W., Combustion optimization of a port-array inverse diffusion flame jet, Energy 36(5) (2011) 2834-2846.
[13] Miller, R.S., Madnia, C.K., and Givi, P., Numerical simulation of non-circular jets, Computers & Fluids 24(1) (1995) 1-25.
[14] GamalEldin, M.A., Ramadan, N.Y., Abdulnaim, A.M., Adam, A.A., Emara, A.A., and Moneib, H.A., Air Jet Assisted Combustion of Oil Diffusion Flames: Effects of Injection Location and Excess Air Factor, Trends in advanced sciences and technology 1(1) (2024).
[15] Elbaz, A.M., Moneib, H.A., Shebil, K.M., and Roberts, W.L., Low NOX - LPG staged combustion double swirl flames, Renewable Energy 138 (2019) 303-315.
[16] Khudhair, R. and Jung, Y., Environmental and Economical Evaluation of Liquified Natural Gas Vehicles Promotion Program in The City of Baghdad, Proceedings of International Exchange and Innovation Conference on Engineering & Sciences (IEICES) 8 (2022) 31-37.
[17] Abdelhameed, E. and Tashima, H., An investigation on the behavior of the torch flame in the LBGE combustion process, Proceedings of International Exchange and Innovation Conference on Engineering & Sciences (IEICES) 8 (2022) 207-214.
[18] A. Mahgoub, A., M. Hussien, A., and A. Emara, K., Experimental Investigation of Stability and Structure of Vertical LPG Inverse Diffusion Flames Issuing from an Elliptic Burner, Engineering Research Journal 171(0) (2021) 119-137.
[19] Mohammed-Taifour, A., Weiss, J., and Dufresne, L., Explicit Algebraic Reynolds-Stress Modeling of Pressure-Induced Separating Flows in the Presence of Sidewalls, Journal of Fluids Engineering 143(10) (2021).
[20] ANSYS CFX-Solver Theory Guide. 2022, ANSYS, Inc.: Canonsburg, PA.